Electronic supporting information

Stable Calcium Ellagate Metal-Organic Framework as High Performance Green Memorizer Bearing High Working Temperature

Ting-Bo Liu,[†a] Jing-Wen Deng,[†b] Yi Li,[c*] Hai-Ying Fu,[d] Liang-Wen Shi,[b] Shi-Ying Lin,[a] Yue Liu,[c] Hao-Hong Li,[c*] Jing-Bo Liu,[b*] and Jian-Zhi Liu[b*]

[a]Fujian Institute of Hematology, Fujian Provincial Key Laboratory of Hematology, Fujian Medical University Union Hospital, Fuzhou, Fujian 350001, P. R. China;

[a]Department of Otorhinolaryngology, Fujian Medical University Union Hospital, Fuzhou, Fujian 350001, P. R. China;

[b]College of Chemistry, Fuzhou University, Fuzhou, Fujian 350108, P. R. China;

[c]Department of Hematology, the Third Affiliated People's Hospital of Fujian University of Traditional Chinese Medicine, the Third People's Hospital of Fujian Province, Fuzhou, Fujian 350108, P. R. China.

[†]T. Liu and J. Deng contributed equally to this work.

Experimental section

Materials and Physical Measurements The starting reagents and solvent (ellagic acid, $Ca(NO_3)_2 \cdot 4H_2O$, DMF) were purchased from Aladdin (Shanghai, China). FT-IR spectrum was recorded on a Perkin-Elmer Spectrum-2000 FTIR spectrophotometer in the range of 4000-400 cm^{-1} using a KBr pellet. UV-visible spectrum was measured on a Shimadzu UV-2600 UV-Vis spectrophotometer (200-800 nm). The optical gaps were calculated from reflectance spectra using the Kubelka−Munk function: $\alpha/s=(1-R)^2/2R$, where α is the absorption coefficient, s is the scattering coefficient, and R is the reflectance.[S1] Powder X-ray diffraction (PXRD) was collected on a Philips X'Pert-MPD diffractometer (Cu Kα radiation, λ=1.54056 Å). TGA was measured on a Mettler Toledo TGA/DSC3+ instrument under an N_2 atmosphere in the temperature range of 30-800°C. HR-SEM images were taken on a Verios G4 field-emission scanning electron microscope. The AFM image was obtained with a ScanAsyst mode on a Bruker Dimension ICON (probe: ScanAsyst-AIR). Current-voltage (*I-V*) characteristics of FTO/$\{[Ca_2(EA)_3(4H_2O)]\cdot 2H_2O\}_n$/Ag device was performed on a KEYSIGHT B2911A source meter.

Synthesis of BioMOF $\{[Ca_2(EA)_3(4H_2O)]\cdot 2H_2O\}_n$ $\{[Ca_2(EA)_3(4H_2O)]\cdot 2H_2O\}_n$ was synthesized with solvothermal method. EA (0.1510 g, 0.5 mmol), $Ca(NO_3)_2 \cdot 4H_2O$ (0.1118 g, 0.5 mmol) were dissolved in 9 mL DMF. The resultant mixture was stirred for 1h at room temperature and then transferred to a 25 mL Teflon-lined autoclave. The system was heated to 150°C in 300 min, and held at this temperature for 72 h. Then the autoclave was cooled to 25°C in 48 h. The block black crystals can be obtained and washed with water and DMF (0.1200 g, yield 43.2 % based on Ca). Anal. Calcd. For $C_{21}H_9CaO_{15}$ (541.36): calcd. C 46.59, H 1.66 O 44.33%; found C 46.41, H 1.56, O 44.62%. IR (cm^{-1}): 3135(s), 1657(w), 1558(s), 1492(s), 1361(s), 1193(s), 1106(s), 1047(w), 833(s), 577(s), 542(s), 456(s).

X-ray single crystal diffraction X-ray diffraction data was collected on a Bruker APEX II CCD area diffractometer equipped with a fine focus, 2.0 kW sealed tube X-ray source (Mo Kα radiation, λ = 0.71073 Å) at room temperature. During the data reduction, multi-scan absorption correction (SADABS) including corrections for Lorentz and polarization effects has applied. Crystal structure was solved by the direct method with program SHELXS and refined with the least-squares program SHELXL.[S2] The structures were verified by the ADDSYM algorithm in the PLATON program.[S3] The refinement details are summarized in Table S1, selected bond lengths and angles are listed in

Table S2, hydrogen bond details and π-π interaction details are given in Table S3 and S4. CCDC 2314792 contains the supplementary crystallographic data for this paper. This data can be obtained free of charge from the Cambridge Crystallographic Data Centre via www.ccdc.cam.ac.uk/data_request/cif.

Device Fabrication The memory device with the structure of FTO/$\{[Ca_2(EA)_3(4H_2O)]\cdot 2H_2O\}_n$/Ag has been fabricated according to previous literature.[S4] The fluorine-doped tin oxide-coated glasses (2 cm × 2 cm, FTO) was pre-cleaned with DMF, ethanol, acetone and deionized water under ultrasonic condition for 30 minutes, then dried at 100°C for 30 min. Afterward, 5 mg as-synthesized BioMOF $\{[Ca_2(EA)_3(4H_2O)]\cdot 2H_2O\}_n$ sample was dissolved in 5 mL DMF (concentration: 1 mg/mL). Then 100 μL as-prepared suspension was spin-coated onto the substrate with FTO as bottom electrode to form BioMOF film. During the spin-coated process, the speed was controlled as follows: 180 rpm for 10 s firstly, and then 1500 rpm for another 30 s. The obtained film was further annealed at 60°C for 1 h on a hotplate. Ag pastes were deposited as the top electrodes through a shadow mask (500 μm width) with circular holes with a diameter about 0.1 cm. Finally, the device was dried at 60°C for 30 minutes to improve the adhesion.

Table S1. Summary of the crystal data and structural determinations.

Empirical formula	$C_{21}H_9CaO_{15}$
Formula mass	541.36
Crystal system	Tetragonal
Space group	$P4_2/ncm$
a[Å]	15.0186(12)
b[Å]	15.0186(12)
c [Å]	18.6119(17)
V[Å]	4198.1(8)
Z	8
D_c[g/cm^3]	1.691
μ[mm^{-1}]	0.385
F(000)	2144
Reflections, total	30362
Reflections, unique	1964 [Rint = 0.0681]
Reflections, observed	1406
Goodness-of-fit on F^2	1.382
R_1[I>2σ(I)]	0.0960
wR_2[I>2σ(I)]	0.3309
Residual extremes(e/Å^3)	1.76/-0.93

Table S2. Selected bonds and angles of $\{[Ca_2(EA)_3(4H_2O)]\cdot 2H_2O\}_n$ (bonds in Å and angles in °)

Bonds	**Length**	**Bonds**	**Length**	**Bonds**	**Length**
Ca(1)-O(1)	2.350(13)	Ca(1)-O(12)	2.64(3)	Ca(1)-O(3)	2.337(14)
Ca(1)-O(4)	2.352(11)	Ca(1)-O(8)	2.439(5)	Ca(1)-O(9)	2.370(5)
Ca(1)-O(8)$^{\#1}$	2.439(5)	Ca(1)-O(9)$^{\#1}$	2.370(5)		
Angle	°	**Angle**	°	**Angle**	°
O(4)-Ca(1)-O(1)	70.1(6)	O(4)-Ca(1)-O(3)	69.0(5)	O(4)-Ca(1)-O(9)$^{\#1}$	136.6(3)
O(1)-Ca(1)-O(3)	139.1(6)	O(1)-Ca(1)-O(9)$^{\#1}$	85.1(4)	O(3)-Ca(1)-O(9)$^{\#1}$	126.2(3)
O(4)-Ca(1)-O(9)	136.6(3)	O(1)-Ca(1)-O(9)	85.0(4)	O(9)$^{\#1}$-Ca(1)-O(9)	72.1(3)
O(3)-Ca(1)-O(9)	126.3(3)	O(4)-Ca(1)-O(8)$^{\#1}$	76.73(14)	O(1)-Ca(1)-O(8)$^{\#1}$	88.20(18)
O(3)-Ca(1)-O(8)$^{\#1}$	82.58(15)	O(9)$^{\#1}$-Ca(1)-O(8)$^{\#1}$	67.21(17)	O(4)-Ca(1)-O(8)	76.69(14)
O(9)-Ca(1)-O(8)$^{\#1}$	139.15(19)	O(1)-Ca(1)-O(8)	88.17(18)	O(3)-Ca(1)-O(8)	82.65(15)
O(9)$^{\#1}$-Ca(1)-O(8)	139.16(19)	O(9)-Ca(1)-O(8)	67.21(17)	O(4)-Ca(1)-O(2)	146.0(11)
O(8)$^{\#1}$-Ca(1)-O(8)	152.8(3)	O(1)-Ca(1)-O(2)	143.9(11)	O(3)-Ca(1)-O(2)	77.0(11)
O(9)$^{\#1}$-Ca(1)-O(2)	66.2(8)	O(9)-Ca(1)-O(2)	66.2(8)		

Symmetry codes: #1 x, y, z

Table S3. π–π stacking interactions in this work (lengths in Å and angles in °)

Cg(I)···Cg(J)	Symmetry code	Dist. Centroids	Dihedral angle	CgI_Perp dist.	CgJ_Perp dist.
Cg(1)→Cg(11)	1-x,-1/2+y,1/2-z	3.751(6)	1.8(4)	3.647(5)	3.6180(16)
Cg(1)→Cg(16)	1-x,-1/2+y,1/2-z	3.656(6)	1.1(4)	3.621(5)	3.6114(14)
Cg(2)→Cg(6)	1-x,1/2+y,1/2-z	3.597(5)	2.2(3)	3.5886(19)	3.595(4)
Cg(2)→Cg(10)	1-x,1-y,1-z	3.648(2)	2.18(18)	3.4404(19)	3.4476(15)
Cg(2)→Cg(13)	1-x,1/2+y,1/2-z	3.717(4)	2.2(3)	3.5886(19)	3.550(4)
Cg(2)→Cg(14)	3/2-x,y,1/2+z	3.638(4)	2.2(2)	3.5886(19)	3.574(4)
Cg(3)→Cg(6)	3/2-x,y,1/2+z	3.597(5)	2.2(3)	3.5884(19)	3.595(4)
Cg(3)→Cg(14)	1/2+x,1-y,1/2-z	3.638(4)	2.2(2)	3.5884(19)	3.574(4)
Cg(3)→Cg(18)	1-x,1-y,1-z	3.670(2)	2.53(17)	3.4050(19)	3.4282(14)
Cg(4)→Cg(16)	x,3/2-y,-1/2+z	3.656(6)	1.1(4)	3.621(5)	3.6114(14)
Cg(5)→Cg(9)	x,3/2-y,-1/2+z	3.627(4)	1.8(3)	3.610(4)	3.6180(16)
Cg(6)→Cg(8)	1-x,-1/2+y,1/2-z	3.741(4)	3.2(3)	3.592(4)	3.6076(15)
Cg(6)→Cg(20)	1-x,-1/2+y,1/2-z	3.727(4)	0.4(3)	3.619(4)	3.6234(14)
Cg(7)→Cg(10)	x,3/2-y,-1/2+z	3.591(5)	0.0(3)	3.591(4)	3.5908(15)
Cg(7)→Cg(16)	1-x,-1/2+y,1/2-z	3.678(5)	1.1(3)	3.599(4)	3.6114(14)
Cg(7)→Cg(20)	x,3/2-y,-1/2+z	3.640(5)	0.4(3)	3.625(4)	3.6234(14)
Cg(8)→Cg(9)	1-x,1-y,1-z	3.683(2)	1.75(14)	3.4117(15)	3.4505(16)
Cg(9)→Cg(10)	1/2-x,3/2-y,z	3.618(2)	1.81(14)	3.4110(16)	3.3911(15)
Cg(9)→Cg(11)	1-x,1-y,1-z	3.393(2)	2.05(14)	3.3886(16)	3.3887(16)
Cg(9)→Cg(13)	1-x,1/2+y,1/2-z	3.627(4)	1.8(3)	3.6181(16)	3.610(4)
Cg(9)→Cg(16)	1-x,1-y,1-z	3.493(2)	0.74(12)	3.3937(16)	3.3912(14)
Cg(10)→Cg(11)	1/2-x,3/2-y,z	3.619(2)	1.81(14)	3.3911(15)	3.4110(16)
Cg(10)→Cg(14)	3/2-x,y,1/2+z	3.656(4)	0.0(2)	3.5907(15)	3.591(4)
Cg(10)→Cg(16)	1/2-x,3/2-y,z	3.488(2)	1.10(12)	3.4288(15)	3.4177(14)
Cg(10)→Cg(18)	x,3/2-y,1/2+z	3.607(4)	0.0(2)	3.5907(15)	3.591(3)

Cg(10)→Cg(19)	3/2-x,y,1/2+z	3.591(4)	0.02(19)	3.5907(15)	3.591(4)
Cg(10)→Cg(20)	1-x,1-y,1-z	3.423(2)	0.35(12)	3.4036(15)	3.4057(14)
Cg(11)→Cg(12)	1-x,1-y,1-z	3.683(2)	1.75(14)	3.4505(16)	3.4118(15)
Cg(11)→Cg(13)	3/2-x,y,1/2+z	3.627(4)	1.8(3)	3.6181(16)	3.610(4)
Cg(11)→Cg(16)	1/2-x,3/2-y,z	3.493(2)	0.74(12)	3.3937(16)	3.3912(14)
Cg(11)→Cg(20)	1-x,1-y,1-z	3.526(2)	1.79(12)	3.3821(16)	3.3548(14)
Cg(12)→Cg(16)	1-x,1-y,1-z	3.727(2)	2.41(12)	3.4270(15)	3.4790(14)
Cg(13)→Cg(16)	x,3/2-y,-1/2+z	3.705(4)	1.1(3)	3.607(4)	3.6114(14)
Cg(13)→Cg(20)	1-x,-1/2+y,1/2-z	3.757(4)	0.4(3)	3.620(4)	3.6234(14)
Cg(14)→Cg(20)	x,3/2-y,-1/2+z	3.643(4)	0.4(2)	3.621(4)	3.6234(14)
Cg(15)→Cg(16)	1-x,-1/2+y,1/2-z	3.780(4)	1.1(2)	3.601(4)	3.6114(14)
Cg(15)→Cg(17)	1-x,-1/2+y,1/2-z	3.703(4)	1.1(2)	3.597(4)	3.6114(14)
Cg(15)→Cg(20)	x,3/2-y,-1/2+z	3.766(4)	0.4(2)	3.630(4)	3.6234(14)
Cg(1+)→Cg(17)	1/2-x,3/2-y,z	3.576(2)	1.99(10)	3.4056(14)	3.4056(14)
Cg(16)→Cg(19)	3/2-x,y,1/2+z	3.678(4)	1.10(17)	3.6114(14)	3.599(4)
Cg(16)→Cg(20)	1-x,1-y,1-z	3.406(2)	0.79(10)	3.3871(14)	3.3896(14)
Cg(17)→Cg(18)	3/2-x,y,1/2+z	3.632(4)	1.1(2)	3.6114(14)	3.605(3)
Cg(17)→Cg(19)	3/2-x,y,1/2+z	3.678(4)	1.10(17)	3.6114(14)	3.599(4)
Cg(17)→Cg(20)	1/2-x,3/2-y,z	3.406(2)	0.79(10)	3.3871(14)	3.3896(14)
Cg(18)→Cg(20)	x,3/2-y,-1/2+z	3.666(4)	0.4(2)	3.626(3)	3.6234(14)
Cg(19)→Cg(20)	x,3/2-y,-1/2+z	3.640(4)	0.35(17)	3.625(4)	3.6234(14)
Cg(20)→Cg(20)	1-x,1-y,1-z	3.3976(19)	0.48(10)	3.3713(14)	3.3712(14)

Ring Cg(1):O(5)→C(10)→C(11)→C(11c)→C(13)→C(12)→

Ring Cg(2):O(10)→C(3)→C(4)→C(4b)→C(6)→C(5)→

Ring Cg(3):C(4)→C(4b)→C(3b)→O(10b)→C(5b)→C(6b)→

Ring Cg(4):C(11)→C(11c)→C(10c)→O(5c)→C(12c)→C(13c)→

Ring Cg(5):O(5)→C(10)→C(9)→C(8)→C(7c)→C(13c)→C(11)→C(11c)→C(13)→C(12)→

Ring Cg(6):O(5)→C(10)→C(11)→C(11c)→C(10c)→C(9c)→C(8c)→C(7)→C(13)→C(12)→

Ring Cg(7):O(5)→C(10)→C(11)→C(13c)→C(12c)→O(5c)→C(10c)→C(11c)→C(13)→C(12)→

Ring Cg(8):O(10)→C(3)→C(2)→C(1)→C(14b)→C(6b)→C(4)→C(4b)→C(6)→C(5)→

Ring Cg(9):O(10)→C(3)→C(4)→C(4b)→C(3b)→C(2b)→C(1b)→C(14) →C(6)→C(5)→

Ring Cg(10):O(10)→C(3)→C(4)→C(6b)→C(5b)→O(10b)→C(3b)→C(4b)→C(6)→C(5)→

Ring Cg(11):C(1)→C(2)→C(3)→C(4)→C(4b)→C(3b)→O(10b)→C(5b)→C(6b)→C(14b)→

Ring Cg(12):C(4)→C(4b)→C(6)→C(14)→C(1b)→C(2b)→C(3b)→O(10b)→C(5b)→C(6b)→

Ring Cg(13):C(7)→C(13)→C(11c)→C(11)→C(13c)→C(12c)→O(5c)→C(10c)→C(9c)→C(8c)→

Ring Cg(14):O(5)→C(10)→C(9)→C(8)→C(7c)→C(13c)→C(12c)→O(5c)→C(10c)→C(11c)→C(13)→C(12)→

Ring Cg(15):O(5)→C(10)→C(11)→C(13c)→C(12c)→O(5c→C(10c)→C(9c)→C(8c)→C(7)→C(13)→C(12)→

Ring Cg(16):O(10)→C(3)→C(2)→C(1)→C(14b)→C(6b)→C(5b)→O(10b)→C(3b)→C(4b)→C(6)→C(5)→

Ring Cg(17):O(10)→C(3)→C(4)→C(6b)→C(5b)→O(10b)→C(3b)→C(2b)→C(1b)→C(14)→C(6)→C(5)→

Ring Cg(18): O(5)→C(10)→C(9)→C(8)→C(7c)→C(13c)→C(1)→C(11c)→C(10c)→C(9c)→C(8c)→C(7)→C(13)→C(12)→

Ring Cg(19):O(5)→C(10)→C(9)→C(8)→C(7c)→C(13c)→C(12c)→O(5c)→C(10c)→C(9c)→C(8c)→C(7)→C(13)→C(12)→

Ring Cg(20):O(10)→C(3)→C(2)→C(1)→C(14b)→C(6b)→C(4)→C(4b)→C(3b)→C(2b)→C(1b)→C(14)→C(6)→C(5)→

Table S4. The comparison of resistive switching parameters with literatures

Devices	V_{Set}/V_{Reset}(V)	ON/OFF ratio	Ref.
Au/HKUST-1/Au/PET	0.76/−0.48	10	S5
Pt/RSMOF-1/W	+7.5/+1.5	30	S6
Ag/Rb-CD-MOF/Ag	2.0/−2.0	1.5×10^2	S7
ITO/POMOF/Ag	1.77/−3.42	10^2	S8
Al/Zn-TCPP@PVPy/ITO	−0.5/2.4	10^3	S9
Ag/MIL-53/GaInSn@PDMS	−1.0/0.4	10^2	S10
Au/ZIF-8/Al	-1.9/2.5	10^4	S11
rGO/MoS_2@ZIF-8/rGO	3.3/−	7.0×10^4	S12
ITO/AuNPs@Cd-MOF-1/ Ag	2.1/−2.1	10^3	S13
ITO/AuNPs@Cd-MOF-1/ Ag	1.5/−2.5	10^4	S13
ITO/AgNPs@Cd-MOF-2/ Ag	4.8/−2.1	10^2	S13
ITO/AgNPs@Cd-MOF-2/ Ag	3.8/−3.8	10^3	S13
FTO/O-MWCNT-CS/Ag	+0.86V/−	$10^{4.51}$	S14
ITO/CS/Cu	+1.6/	10^3	S15
Ag/Au-chitosan/Au	+2.5/-2.5	10^2	S16
FTO/$\{[Ca_2(EA)_3(4H_2O)]\cdot2H_2O\}_n$ /Ag	1.12/-4.54	5.40×10^3	This work

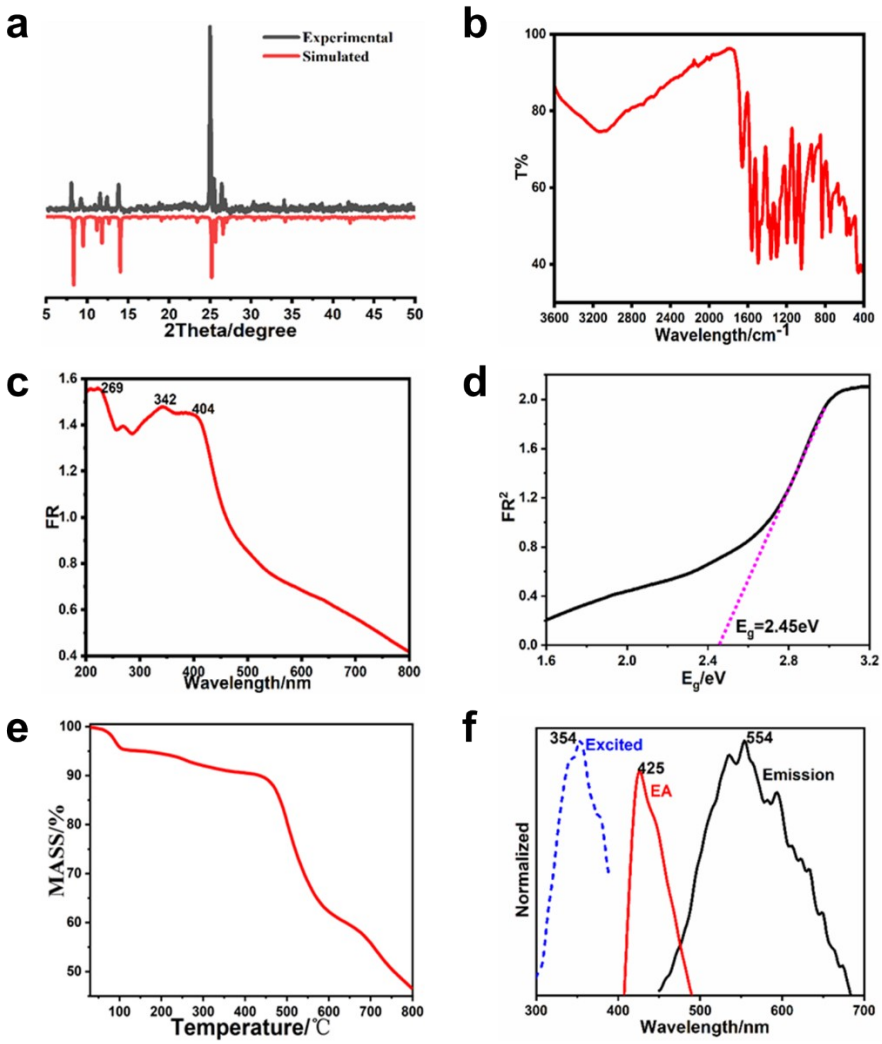

Fig. S1. Characterizations of $\{[Ca_2(EA)_3(4H_2O)]\cdot 2H_2O\}_n$: (a) PXRD; (b) FT-IR spectrum; (c) UV-Vis diffuse reflection spectrum; (d) optical gap calculated from Kubelka−Munk function; (e) TG curve; (f) solid state photoluminescence spectrum.

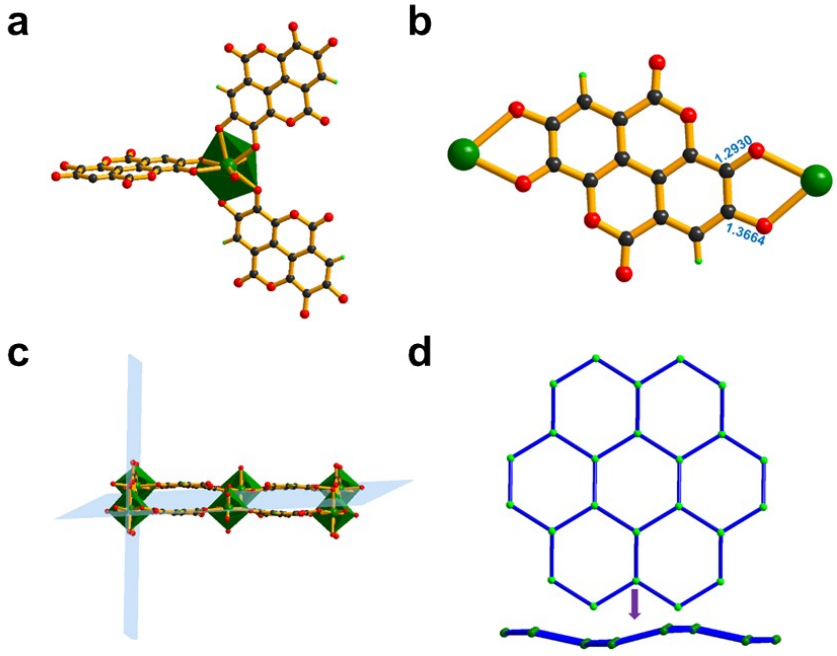

Fig. S2. (a) Coordinated environment of Ca atom; (b) coordinated mode of EA ligand; (c) the dihedral angle between two crystallographically independent EA ligands; (d) wave-like (6,3) topology of $[Ca_2(EA)_3(4H_2O)]_n$ layer.

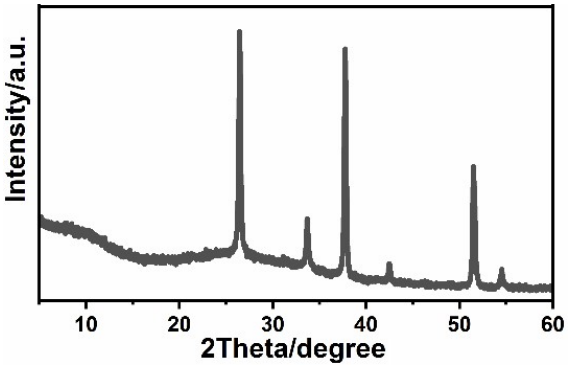

Fig. S3. PXRD patterns of FTO/BioMOF film.

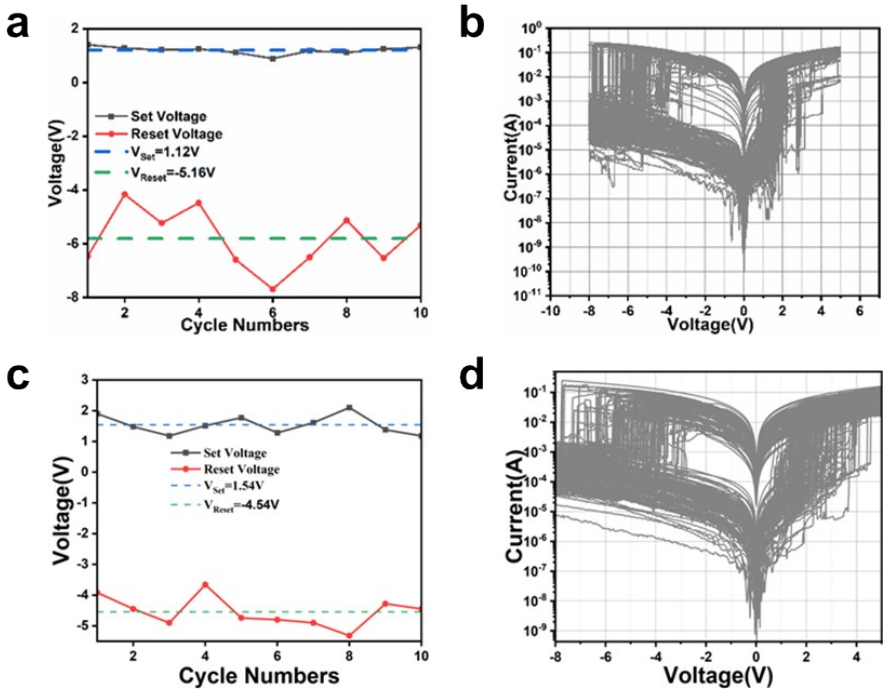

Fig. S4. (a) V_{Set}/V_{Reset} distribution showing 10 random cycles at room temperature; (b) *I-V* curves showing 100 cycles at room temperature; (c) V_{Set}/V_{Reset} distribution showing 10 random cycles at 300 ˚C; (d) *I-V* curves showing 100 cycles at 300 ˚C.

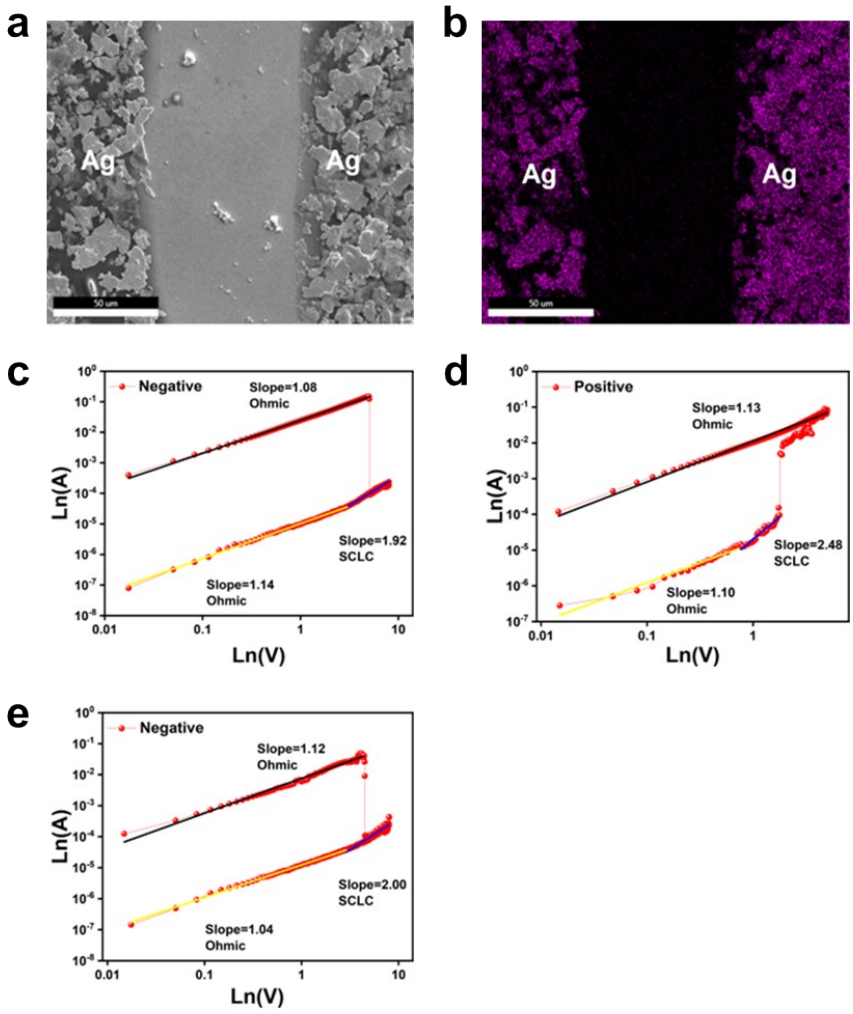

Fig. S5. (a) FIB SEM image of Ag/{$[Ca_2(EA)_3(4H_2O)]\cdot 2H_2O\}_n$/Ag model device before set operation; (b) Ag mapping before set operation; (c) ln-ln plot on the *I-V* curve under negative voltage sweep at room temperature; (d, e) ln-ln plot on the *I-V* curve under positive/negative voltage sweep at 300 ˚C.

References

[S1] P. Makula, M. Pacia and W. Macyk, How to correctly determine the band gap energy of modified semiconductor photocatalysts based on UV–Vis spectra，*J. Phys. Chem. Lett.* 2018, **9**, 6814–6817.

[S2] G. A. Sheldrick, A short history of SHELX, *Acta Crystallogr. Sect. A* 2008, **64**, 112–122.

[S3] A. Spek, Single-crystal structure validation with the program PLATON, *J. Appl. Crystallogr.* 2003, **36,** 7–13.

[S4] K. Song, B. Chen, X. Lin, H. Yang, Y. Liu, H. Li and Z. Chen, Thermal enhanced resistive switching performance of<100>-oriented perovskite $[(TZ\text{-}H)_2(PbBr4)]_n$ with high working temperature: a triazolium/$(PbBr_4)_n^{2n-}$ interfacial interaction insight, *Adv. Electron. Mater.* 2022, **8**, 2200537.

[S5] L. Pan, Z. Ji, X. Yi, X. Zhu, X. Chen, J. Shang, G. Liu and R. W. Li, Metal-organic framework nanofilm for mechanically flexible information storage applications, *Adv. Funct. Mater.* 2015, **25**, 2677–2685.

[S6] L. Pan, G. Liu, H. Li, S. Meng, L. Han, J. Shang, B. Chen, A. E. Platero-Prats, W. Lu, X. Zou and R. W. Li, A Resistance-switchable and ferroelectric metal–organic framework, *J. Am. Chem. Soc.* 2014, **136**, 17477–17483.

[S7] S. M. Yoon, S. C. Warren and B. A. Grzybowski, Storage of electrical information in metal–organic-framework memristors, *Angew. Chem., Int. Ed.* 2014, **53**, 4437–4441.

[S8] B. Chen, Y. Huang, K. Song, X. Lin, H. Li and Z. Chen, Molecular nonvolatile memory based on [α-$GeW_{12}O_{40}]^{4-}$/metalloviologen hybrids can work at high temperature monitored by chromism, *Chem. Mater.* 2021, **33**, 2178−2186.

[S9] G. Ding, Y. Wang, G. Zhang, K. Zhou, K. Zeng, Z. Li, Y. Zhou, C. Zhang, X. Chen and S. T. Han, 2D metal-organic framework nanosheets with time-dependent and multilevel memristive switching, *Adv. Funct. Mater.* 2019, **29**, 1806637.

[S10] X. Yi, Z. Yu, X. Niu, J. Shang, G. Mao, T. Yin, H. Yang, W. Xue, P. Dhanapal, S. Qu, G. Liu and R. W. Li, Intrinsically stretchable resistive switching memory enabled by combining a liquid metal–based soft electrode and a metal–organic framework insulator, *Adv. Electron. Mater.* 2019, **5,** 1800655.

[S11] M.-J. Park and J.-S. Lee, Zeolitic-imidazole framework thin film-based flexible resistive switching memory, *RSC Adv.* 2017, **7**, 21045–21049.

[S12] Y. Liu, H. Wang, W. Shi, W. Zhang, J. Yu, B. K. Chandran, C. Cui, B. Zhu, Z. Liu, B. Li, C. Xu, Z. Xu, S. Li, W. Huang, F. Huo and X. Chen, Alcohol-mediated resistance-switching behavior in metal–organic framework-based electronic devices, *Angew. Chem., Int. Ed.* 2016, **55**, 8884–8888.

[S13] L. Zhao, W. Wu, X. Shen, Q. Liu, Y. He, K. Song, H. Li and Z. Chen, Nonvolatile electrical bistability behaviors observed in Au/Ag nanoparticle-embedded MOFs and switching mechanisms, *ACS Appl. Mater. Interfaces*, 2019, **11**, 47073−47082.

[S14] H. Yi, G. Yu, Z. Lv, H. Li, X. Lin, H. Li and H. Zheng, Simultaneously elevating the resistive switching performance and thermal/irradiative stabilities of biomemorizer based on twisted carboxylated multi-walled carbon nanotube-chitosan composites, *J. Alloy Compd.* 2023, **952**, 169934.

[S15] M.R. Kiran, Y. Yadav and S.P. Singh, Chitosan based memory devices: filamentary versus interfacial resistive switching, *J. Phys. D: Appl. Phys*. 2022, **55**, 055302.

[S16] N. Raeis-Hosseini and J. Rho, Solution-processed flexible biomemristor based on gold-decorated chitosan, *ACS. Appl. Mater. Interfaces.* 2021, **13**, 5445–5450.